

Active Screws: Emergent Active Chiral Nematics of Spinning Self-Propelled Rods

Debarghya Banerjee¹ and Ricard Alert^{2,3,4,*}

¹*Institute for Theoretical Physics, Georg-August-Universität Göttingen, 37077 Göttingen, Germany*

²*Max Planck Institute for the Physics of Complex Systems, Nöthnitzerstr. 38, 01187 Dresden, Germany*

³*Center for Systems Biology Dresden, Pfotenhauerstr. 108, 01307 Dresden, Germany*

⁴*Cluster of Excellence Physics of Life, TU Dresden, 01062 Dresden, Germany*

(Dated: October 17, 2024)

Several types of active agents self-propel by spinning around their propulsion axis, thus behaving as active screws. Examples include cytoskeletal filaments in gliding assays, magnetically-driven colloidal helices, and microorganisms like the soil bacterium *M. xanthus*. Here, we develop a model for spinning self-propelled rods on a substrate, and we coarse-grain it to derive the corresponding hydrodynamic equations. If the rods propel purely along their axis, we obtain equations for a dry active nematic. However, spinning rods can also roll sideways as they move. We find that this transverse motion turns the system into a chiral active nematic. Thus, we identify a mechanism whereby individual chirality can give rise to collective chiral flows. Finally, we analyze experiments on *M. xanthus* colonies to show that they exhibit chiral flows around topological defects, with a chiral activity about an order of magnitude weaker than the achiral one. Our work reveals the collective behavior of active screws, which is relevant to colonies of social bacteria and groups of unicellular parasites.

Across scales, Nature has taken advantage of the principle of a screw to drive motion. At the molecular scale, in so-called gliding assays, both microtubules and actin filaments are propelled and spun by carpets of molecular motors¹. At the cellular scale, rod-shaped bacteria like *Myxococcus xanthus* and *Flavobacterium johnsoniae* glide on surfaces by spinning around their body axis²⁻⁹. Other bacteria, like *Treponema primitia* swim by spinning their helical bodies². At larger scales, starfish embryos¹⁰ and algae like *Chlamidomonas reinhardtii*¹¹ and *Volvox*¹² also swim while spinning. Beyond the living world, screw-like propulsion was achieved in synthetic helical micropropellers driven by magnetic fields¹³⁻¹⁵ or chemical reactions^{15,16}, and it was also found in simulations of active droplets^{17,18}. All these systems share a key feature: Self-propulsion and spinning share the same axis, and the self-propulsion speed is proportional to the spinning rate. These systems therefore behave as active screws.

In contrast, most work on active chiral particles has focused on objects on a plane that spin around the axis perpendicular to the plane¹⁹⁻²¹ (Figs. 1a and 1b). Systems with this type of chiral motion include bacterial and sperm cells close to surfaces²²⁻²⁶, microtubules²⁷, FtsZ filaments²⁸, as well as L-shaped self-propelled colloids²⁹ and magnetic spinners^{30,31}. Another class of spinning active particles are rollers, such as Quincke rollers³², which spin around an axis in the same plane but perpendicular to the self-propulsion axis (Fig. 1c). In all these cases, the axes of rotation and translation are different. Here, we introduce *active screws* as a class of active particles for which the axes of rotation and translation are the same (Fig. 1d).

Rotation and translation along the same axis are common in microswimmers, for example in bacteria propelled by helical flagella. In that case, however, the swimmer is torque-free, and hence the rotation of the flagella is compensated by a counter-rotation of the cell body^{2,33,34}. The swimmer therefore experiences no net rotation, and it exerts a torque dipole.

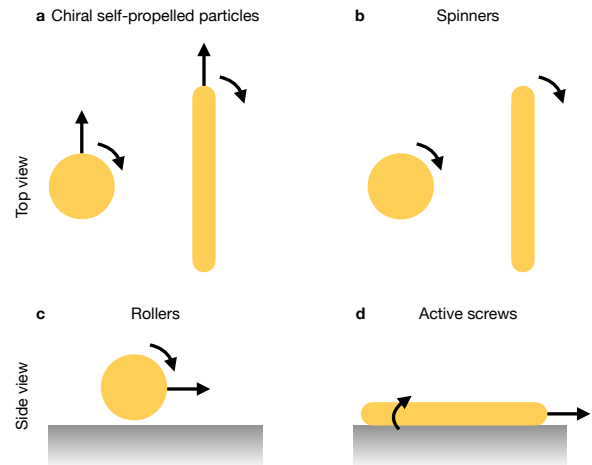


Figure 1 | Classes of active chiral particles. **a**, Chiral self-propelled particles propelling on the plane and spinning around the axis perpendicular to it. **b**, Spinners do not translate. **c**, Rollers spin around an in-plane axis perpendicular to their self-propulsion. **d**, Active screws spin and self-propel along the same axis.

In contrast, we focus on active screws moving on surfaces, such as gliding bacteria, which rotate their entire body in the same direction and are therefore driven by a torque monopole. Recent work started to describe the intracellular flows that power this type of gliding motility^{35,36}. However, perhaps with the exception of the vortices formed by crescent-shaped malaria parasites³⁷, the collective behavior of active screws remains largely unaddressed.

Here, we develop a microscopic model of active screws and we coarse-grain it to obtain the continuum equations that capture their collective behavior. Our results show that, if active screws propel purely along their axis, they form an active nematic. The theory of active nematics was recently used to explain cell flows and the formation of cell layers in colonies of *M. xanthus*^{38,39}. However, the connection between the con-

* ralert@pks.mpg.de

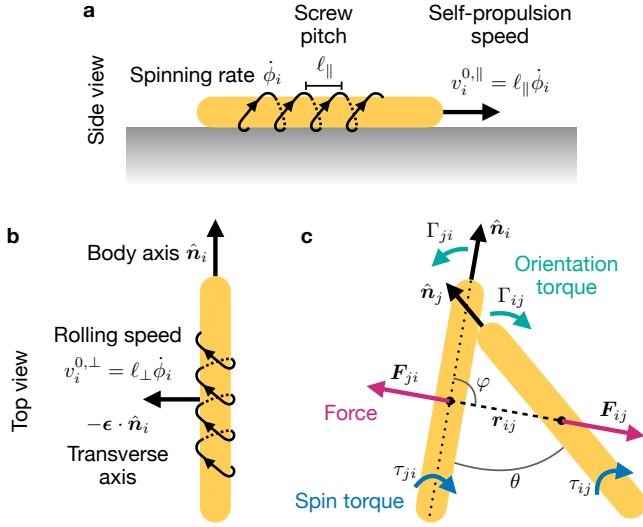


Figure 2 | Motion and interactions of active screws. **a**, An active screw spinning at a rate $\dot{\phi}_i$ with a pitch ℓ_{\parallel} propels along its axis at a speed $v_i^{0,\parallel} = \ell_{\parallel} \dot{\phi}_i$. **b**, An active screw can also propel sideways by rolling at a speed $v_i^{0,\perp} = \ell_{\perp} \dot{\phi}_i$. **c**, The interactions between active screws include forces, torques that change their orientations, and torques that change their spinning rate.

tinuum equations and the microscopic dynamics of this gliding bacterium was not established. Our results provide this connection: We give the coefficients of the continuum theory in terms of the microscopic parameters. Finally, we generalize our findings to active screws that also roll sideways, thus adding a transverse component of motion. In this case, we obtain the equations of chiral active nematics. We thus identify a mechanism whereby the chirality of individual constituents can give rise to collective chiral effects. Overall, our work generalizes the theory of self-propelled rods^{40,41} to spinning particles, and it can be tested in colonies of gliding bacteria.

Microscopic model of active screws. We model the spinning of active screws via their spinning rate $\dot{\phi}_i$ as (Fig. 2a):

$$\dot{\phi}_i = \omega \Phi_i(t) + \frac{\tau_i}{\xi_s}. \quad (1)$$

The first term accounts for self-spinning at a rate ω . Moreover, gliding bacteria experience stochastic spinning reversals⁴². We include them via a dichotomous noise $\Phi_i(t)$ that switches between +1 and -1 with Poisson statistics, such that $\langle \Phi_i(t) \Phi_j(t') \rangle = \delta_{ij} \exp(-2f_{\text{rev}}|t - t'|)$, where f_{rev} is the average reversal frequency. Similar to a recent model for eukaryotic cell doublets⁴³, the second term accounts for spin torque transfer between neighboring screws (blue in Fig. 2c), $\tau_i = \sum_{j \neq i} \tau_{ji}$, which affects the spinning rate through the spin friction coefficient ξ_s . We assume a torque transfer proportional to the relative velocity between the rod surfaces, and hence to the sum of their spinning rates: $\tau_{ij} = \tau_r(r)(\dot{\phi}_i + \dot{\phi}_j) \cos \theta$, where $r = |\mathbf{r}_{ij}|$ is the distance and $\cos \theta = \hat{\mathbf{n}}_i \cdot \hat{\mathbf{n}}_j$ is the projection between the two rods (Fig. 2c).

We then describe screw motion by coupling the spinning

rate to translation, such that the self-propulsion speed of rod i along its axis is $v_i^{0,\parallel} = \ell_{\parallel} \dot{\phi}_i$. Here, ℓ_{\parallel} is the pitch of the screw, i.e., the distance it advances in one revolution (Fig. 2a). We also allow the rods to roll sideways as a result of their spinning, moving at a speed $v_i^{0,\perp} = \ell_{\perp} \dot{\phi}_i$ perpendicularly to the rod axis $\hat{\mathbf{n}}_i \equiv (\cos \theta_i, \sin \theta_i)$, where ℓ_{\perp} is the rolling pitch (Fig. 2b). If rolling occurs without slipping, then $\ell_{\perp} = 2\pi R$, with R the rod radius. Thus, the rod positions \mathbf{r}_i follow

$$\frac{d\mathbf{r}_i}{dt} = \ell_{\parallel} \dot{\phi}_i \hat{\mathbf{n}}_i - \ell_{\perp} \dot{\phi}_i \epsilon \cdot \hat{\mathbf{n}}_i + \frac{\mathbf{F}_i}{\xi_t}, \quad (2)$$

where ϵ is the Levi-Civita symbol, and $\mathbf{F}_i = \sum_{j \neq i} \mathbf{F}_{ji}$ is the force of interaction with neighboring rods, which changes rod positions through the translational friction coefficient ξ_t . We assume the force between two rods to be central, and proportional to their projection: $\mathbf{F}_{ij} = F_r(r) \cos \theta \hat{\mathbf{r}}_{ij}$ (purple in Fig. 2c). Brownian motion is typically negligible in gliding cells since they are well attached to the substrate. Therefore, we ignore translational noise.

Finally, the orientation angle of the rods evolves as

$$\frac{d\theta_i}{dt} = \frac{\Gamma_i}{\xi_r} + \eta_i^r(t), \quad (3)$$

where $\Gamma_i = \sum_{j \neq i} \Gamma_{ji}$ is the orientation torque from interactions with other rods (green in Fig. 2c), which affects angle through the rotational friction coefficient ξ_r , and $\eta_i^r(t)$ is a Gaussian noise with strength given by the rotational diffusivity D_r : $\langle \eta_i^r(t) \eta_j^r(t') \rangle = 2D_r \delta(t - t') \delta_{ij}$. We assume nematic orientational interactions: $\Gamma_{ij} = \Gamma_r(r) \sin(2\theta)$ (Fig. 2c). Unlike for other classes of active chiral particles (Figs. 1a and 1b), here we introduce no self-rotation in the orientation angle θ_i .

Coarse-graining and hydrodynamic equations. To predict the collective behavior of active screws, we coarse-grain the set of Langevin equations Eqs. (1) to (3). First, we eliminate Eq. (1) by introducing it into Eq. (2). However, this does not eliminate the spinning rate $\dot{\phi}_i$ as a degree of freedom, as the spin torque transfer τ_{ij} still depends on it. Respectively, the stochastic reversals encoded in $\Phi_i(t)$ give rise to an effective rotational diffusivity⁴⁴ $D_r^{\text{eff}} = D_r + 2f_{\text{rev}}$ on time scales $t \gg f_{\text{rev}}^{-1}$. Second, for this reduced set of Langevin equations, we write the corresponding Smoluchowski equation and we break it into the Bogoliubov-Born-Green-Kirkwood-Yvon (BBGKY) hierarchy to obtain an equation for the one-particle distribution function $\Psi_1(\mathbf{r}_1, \theta_1, \dot{\phi}_1, t)$ (SI Section I). From it, we obtain hydrodynamic equations for the density, polarity, and nematic order parameter fields, $\rho(\mathbf{r}, t)$, $\mathbf{p}(\mathbf{r}, t)$, and $\mathbf{Q}(\mathbf{r}, t)$, respectively (SI Section I), which we present and discuss below. We obtain the equations in the nematic state, in which the angle between rods is $\theta \approx 0$.

For the rod density field, we obtain

$$\partial_t \rho = -\nabla \cdot \mathbf{J}; \quad \mathbf{J} = v_{\parallel}[\rho] \mathbf{p} - v_{\perp} \epsilon \cdot \mathbf{p} - \zeta_1 \rho \nabla \rho. \quad (4)$$

The first term in the flux \mathbf{J} is advection along the polarity field $\mathbf{p}(\mathbf{r}, t)$ at a local speed $v_{\parallel}[\rho] = \omega \ell_{\parallel} - \zeta_0 \rho$. This speed is produced by the screw motion at a self-spinning rate ω_0 ,

and it decreases with the density field $\rho(\mathbf{r}, t)$. The coefficient ζ_0 , given in Eq. (S18), captures the slowdown resulting from repulsive interactions between rods, which is responsible for motility-induced phase separation^{45,46}. The second term in Eq. (4) corresponds to a flux perpendicular to the polarity at a speed $v_\perp = \omega \ell_\perp$ driven by rolling motion. The transverse speed v_\perp does not have a slowdown effect because we assume that the system is statistically achiral, and hence the repulsive forces from the right and the left of a reference rod cancel out. Finally, the last term in Eq. (4), with ζ_1 given in Eq. (S23), is a diffusive flux induced by repulsive interactions between rods⁴⁷.

The polarity field follows the following equation:

$$\begin{aligned} \partial_t \mathbf{p} = & -\nabla \cdot (v_{\parallel}[\rho] \mathbf{Q}) - \frac{1}{2} \nabla (v_{\parallel}[\rho] \rho) + \nabla \cdot (v_\perp \boldsymbol{\epsilon} \cdot \mathbf{Q}) \\ & + \frac{1}{2} \boldsymbol{\epsilon} \cdot \nabla (v_\perp \rho) + \nabla \cdot (\zeta_1 \mathbf{p} \nabla \rho) - D_r^{\text{eff}} \mathbf{p}. \end{aligned} \quad (5)$$

This result shows that, to lowest order in gradients and at times $t \gg 1/D_r^{\text{eff}}$, the polarity field has contributions from the divergence of the nematic order-parameter tensor \mathbf{Q} and from density gradients. Due to self-propulsion, this polarity then produces density currents in Eq. (4), which are a key ingredient of dry active nematics^{40,48}. In the presence of rolling, with $v_\perp \neq 0$, the polarity gets additional transverse contributions represented by the third and fourth terms in Eq. (5).

The density current relates to the velocity field $\mathbf{v}(\mathbf{r}, t)$ as $\mathbf{J} = \rho \mathbf{v}$. For a system with uniform density $\rho = \rho_0$, using the steady-state solution of Eq. (5), we obtain a velocity field that corresponds to that produced by active stresses of a chiral nematic on a substrate^{49–52}:

$$\mathbf{v} = \frac{1}{\xi} \nabla \cdot \boldsymbol{\sigma}_{\text{act}}; \quad \boldsymbol{\sigma}_{\text{act}} = -\zeta \mathbf{Q} + \zeta_c \boldsymbol{\epsilon} \cdot \mathbf{Q}. \quad (6)$$

Here, following the convention in the field, we take \mathbf{Q} to be the dimensionless nematic order parameter, whereas \mathbf{Q} in Eq. (5) is its density, with units of squared inverse length. In Eq. (6), ξ is the friction coefficient, and ζ and ζ_c are the coefficients for achiral and chiral active stresses, respectively. Our results relate these coefficients to the parameters of the active-screw model as

$$\frac{\zeta}{\xi} = \frac{v_{\parallel}^2 - v_\perp^2}{D_r^{\text{eff}}}, \quad \frac{\zeta_c}{\xi} = \frac{2v_{\parallel}v_\perp}{D_r^{\text{eff}}}, \quad (7)$$

where we simplify notation by using $v_{\parallel} \equiv v_{\parallel}[\rho_0]$.

Finally, the equation for the nematic order-parameter field reads

$$\begin{aligned} \partial_t Q_{\alpha\beta} = & -\partial_\gamma (v_{\parallel}[\rho] T_{\alpha\beta\gamma}) + \delta_{\alpha\beta} \partial_\gamma \left(\frac{v_{\parallel}[\rho]}{2} p_\gamma \right) \\ & + \partial_\gamma (v_\perp \epsilon_{\gamma\mu} T_{\alpha\beta\mu}) - \partial_\gamma \left(\frac{v_\perp}{2} \delta_{\alpha\beta} \epsilon_{\gamma\mu} p_\mu \right) \\ & + \partial_\gamma (\zeta_1 Q_{\alpha\beta} \partial_\gamma \rho) - D_r^{\text{eff}} Q_{\alpha\beta}. \end{aligned} \quad (8)$$

Here, $T_{\alpha\beta\gamma}$ is the third-rank orientational tensor (SI Section I). Equation (8) shows that the nematic order parameter has active contributions due to screw motion as well as the corresponding transverse contributions due to rolling. In the absence of activity, the nematic order parameter relaxes to zero

by virtue of the rotational noise captured in D_r^{eff} . Therefore, our microscopic model can produce activity-driven nematic order if either the third-rank orientational tensor or the polarity do not vanish. This result is consistent with previous works on self-propelled rods, which found that activity decreases the threshold for the isotropic-nematic transition^{40,53,54}. Our possibility of activity-induced order, however, contrasts with most models of active nematics, for which nematic order is incorporated directly in the free energy as it is assumed to arise from the passive alignment interactions between the constituents⁴⁰. Moreover, our system is dry, meaning that friction completely screens hydrodynamic interactions. Thus, the possibility for activity-driven nematic order in our system is different from a recently-predicted instability whereby isotropic wet active nematics can order due to a feedback between active flows and nematic order⁵⁵.

Regarding chiral effects, Eq. (8) lacks the term $\sim \Omega \epsilon_{\alpha\gamma} Q_{\gamma\beta}$ describing the self-rotation of the axis of nematic order introduced in previous works on chiral active nematics⁵¹. This difference is because, in contrast to previous models of chiral active rods (Fig. 1a), active screws spin around the orientation axis (Fig. 1d), which therefore does not self-rotate.

Chiral flows around topological defects. We compare the predictions of our theory to recent measurements of flow fields around topological defects in colonies of the gliding, spinning bacterium *M. xanthus*^{38,39}. Fitting the continuum theory of active nematics to the experimental data gave values of $\zeta/\xi \approx 2 \mu\text{m}^2/\text{min}$ ³⁸. Here, ignoring rolling ($v_\perp = 0$), we use independent measurements of the self-propulsion speed^{44,56}, $v_{\parallel} = 1.3 \mu\text{m}/\text{min}$, and of the effective rotational diffusivity⁴⁴, $D_r^{\text{eff}} = 0.34 \text{ min}^{-1}$, to predict $\zeta/\xi \approx 5 \mu\text{m}^2/\text{min}$ from Eq. (7). This value, predicted from our microscopic model, is slightly larger but comparable with the fit results to experimental data.

Next, we consider the effects of rolling ($v_\perp \neq 0$), which give rise to chiral flows. Chiral flows around defects have been previously proposed to arise in fibrosarcoma cell layers^{57,58}. Here, we analyzed the experimental data in Fig. 4 of Ref.³⁸ and we found that the flows have a non-zero chiral component. For defects oriented along the \hat{x} axis, as in the schematics in Fig. 3, chiral flows are revealed by a non-zero average velocity along the \hat{y} axis: $\langle v_y \rangle \neq 0$. For $+1/2$ defects, we compute the average velocity in a circle of radius R centered at the defect. For $R = 5 \mu\text{m}$ and $R = 10 \mu\text{m}$, we obtain a ratio of velocity components in the range $\langle v_y \rangle_R / \langle v_x \rangle_R \approx 0.15 - 0.19$, showing that the chiral flows are approximately six times weaker than the achiral ones. Solving our model Eq. (6), even including anisotropic friction^{38,59}, gives $\langle v_y \rangle_R / \langle v_x \rangle_R = \zeta_c / \zeta$ (SI Section II). Hence, we estimate $\zeta_c / \zeta \approx 0.15 - 0.19$, which, using $\zeta/\xi \approx 2 \mu\text{m}^2/\text{min}$ ^{38,39}, implies $\zeta_c / \xi \approx 0.30 - 0.38 \mu\text{m}^2/\text{min}$. We then use Eq. (7) and the values of v_{\parallel} and D_r^{eff} listed above to obtain a value for the rolling speed $v_\perp \approx 0.04 - 0.05 \mu\text{m}/\text{min}$. The flow fields predicted by the theory are shown in Fig. 3, with all the parameter estimates gathered in Table I.

Our analysis revealed chiral flows around topological defects in colonies of *M. xanthus*. While our theory does not attempt to achieve quantitative agreement with the experiments, it identifies a possible mechanism for the chiral flows: The

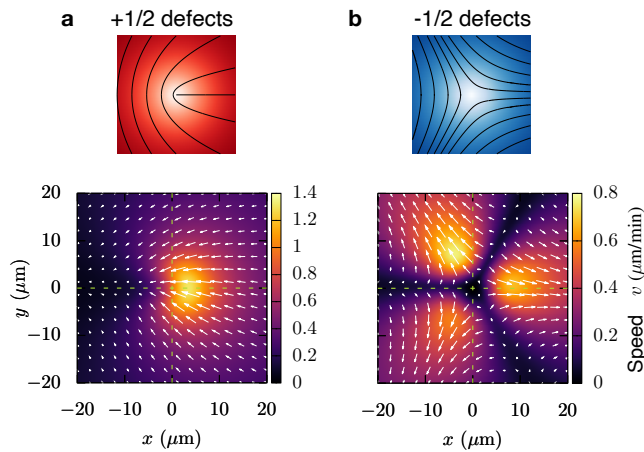


Figure 3 | Chiral flows around topological defects. Defect schematics (top) show the order parameter (color) and the director field (lines). The flow fields (bottom) predicted by our theory (Eq. (6)) are slightly chiral. The solutions for the flow field are given in SI Section II, and the parameter values are listed in Table I.

Symbol	Description	Estimate
S_0	Strength of nematic order	0.992 (Ref. ³⁸)
ℓ	Nematic healing length (core size)	$2.5 \mu\text{m}$ (Ref. ³⁸)
ζ/ξ	Active stress / friction	$2 \mu\text{m}^2/\text{min}$ (Ref. ³⁸)
ε	Friction anisotropy	0.7 (Ref. ³⁸)
D_r^{eff}	Effective rotational diffusivity	0.34 min^{-1} (Ref. ⁴⁴)
v_{\parallel}	Longitudinal self-propulsion speed	$1.3 \mu\text{m}/\text{min}$ (Ref. ^{44,56})
ζ_c/ζ	Chiral / achiral active stress	0.17
ζ_c/ξ	Chiral active stress / friction	$0.34 \mu\text{m}^2/\text{min}$
v_{\perp}	Rolling speed	$0.045 \mu\text{m}/\text{min}$

Table I | Parameter estimates for the bacterium *M. xanthus*. The last three estimates are obtained in this work.

rolling motion of bacteria due to their spinning-based gliding motility. Rolling was achieved in helical microswimmers⁶⁰. Although we know of no direct evidence for rolling in gliding bacteria, our results suggest that chiral cellular flows around defects might be an indirect evidence for this type of cellular motion. Our estimates indicate that the rolling speed could be more than an order of magnitude smaller than the longitudinal self-propulsion speed. Hence, rolling might have been overlooked in the experiments. Based on these findings, future experiments can both search for direct evidence of rolling and investigate alternative mechanisms for chiral flows.

Discussion and outlook. We introduced a microscopic model for active screws — a class of active chiral particles that spin around their axis of self-propulsion (Fig. 1d). Compared to other classes of active particles, which are described by their position and orientation, active screws have an additional degree of freedom: their spinning rate. The spinning rate contributes to (i) the speed at which active screws propel themselves forwards, (ii) the speed at which they roll sideways, and (iii) the spin torque transferred among neighboring screws. Whereas previously-studied active chiral particles also spin, they do it perpendicularly to their axis of self-propulsion (Figs. 1a to 1c). Moreover, in most cases studied so far, the spinning rate was constant, independent of the self-propulsion speed and of interactions with other particles. Hence, the spinning rate was so far a parameter instead of a degree of freedom as in the case of active screws.

We predicted the collective behavior of active screws by coarse-graining the microscopic model. We obtained continuum equations that correspond to a chiral active nematic, showing how the screw and rolling motion give rise to achiral and chiral active nematic stresses, respectively. These results establish a connection between the parameters of the microscopic model and those of the macroscopic continuum equations. This micro-macro connection is directly relevant for colonies of gliding bacteria, where single-cell decisions are thought to control collective behaviors^{44,61,62}.

We then analyzed experimental data from Ref.³⁸ to reveal the presence of chiral flows in colonies of *M. xanthus*. We estimated the corresponding active chiral stresses to be an order of magnitude weaker than the achiral ones. Using the micro-macro connection, we estimated the values of microscopic parameters, such as the rolling speed, from experimental data. Our results could potentially also explain collective chiral flows observed in colonies of other bacteria with screw-like propulsion, such as *C. gingivalis*⁶³ and *F. johnsoniae*⁶⁴. Overall, using our theory of active screws, we propose that a possible mechanism for emergent chiral flows is the transverse rolling motion that can take place when a screw spins against a substrate. We propose to test these ideas against possible alternative mechanisms in future experiments.

Acknowledgments

R.A. thanks Sagnik Garai, Stephan Grill, Pierre Haas, Christina Kurzthaler, David Oriola, and Joshua Shaevitz for discussions. R.A. thanks the Isaac Newton Institute for Mathematical Sciences for the support and hospitality during the programme *Anti-diffusive dynamics: from sub-cellular to astrophysical scales*, supported by EPSRC Grant Number EP/R014604/1, when work on this paper was undertaken.

1. Laura Meißner, Lukas Niese, and Stefan Diez, “Helical motion and torque generation by microtubule motors,” *Curr. Opin. Cell Biol.* **88**, 102367 (2024).
2. Navish Wadhwa and Howard C. Berg, “Bacterial motility: machinery and mechanisms,” *Nat. Rev. Microbiol.* **20**, 161–173

(2022).

3. Tãm Mignot, Joshua W. Shaevitz, Patricia L. Hartzell, and David R. Zusman, “Evidence That Focal Adhesion Complexes Power Bacterial Gliding Motility,” *Science* **315**, 853–856 (2007).

4. Rajesh Balagam, Douglas B. Litwin, Fabian Czerwinski, Mingzhai Sun, Heidi B. Kaplan, Joshua W. Shaevitz, and Oleg A. Igoshin, “Myxococcus xanthus Gliding Motors Are Elastically Coupled to the Substrate as Predicted by the Focal Adhesion Model of Gliding Motility,” *PLoS Comput. Biol.* **10**, e1003619 (2014).
5. Laura M. Faure, Jean-Bernard Fiche, Leon Espinosa, Adrien Ducret, Vivek Anantharaman, Jennifer Luciano, Sébastien Lhospice, Salim T. Islam, Julie Tréguier, Mélanie Sotes, Erkin Kuru, Michael S. Van Nieuwenhze, Yves V. Brun, Olivier Théodoly, Aravind L. Marcelo Nollmann, and Târn Mignot, “The mechanism of force transmission at bacterial focal adhesion complexes,” *Nature* **539**, 530–535 (2016).
6. Daisuke Nakane, Keiko Sato, Hirofumi Wada, Mark J. McBride, and Koji Nakayama, “Helical flow of surface protein required for bacterial gliding motility,” *Proc. Natl. Acad. Sci. U. S. A.* **110**, 11145–11150 (2013).
7. Abhishek Shrivastava, Pushkar P. Lele, and Howard C. Berg, “A Rotary Motor Drives Flavobacterium Gliding,” *Curr. Biol.* **25**, 338–341 (2015).
8. Abhishek Shrivastava and Howard C. Berg, “Towards a model for Flavobacterium gliding,” *Curr. Opin. Microbiol.* **28**, 93–97 (2015).
9. Abhishek Shrivastava, Thibault Roland, and Howard C. Berg, “The Screw-Like Movement of a Gliding Bacterium Is Powered by Spiral Motion of Cell-Surface Adhesins,” *Biophys. J.* **111**, 1008–1013 (2016).
10. Tzer Han Tan, Alexander Mietke, Junang Li, Yuchao Chen, Hugh Higinbotham, Peter J. Foster, Shreyas Gokhale, Jörn Dunkel, and Nikta Fakhri, “Odd dynamics of living chiral crystals,” *Nature* **607**, 287–293 (2022).
11. Dario Cortese and Kirsty Y. Wan, “Control of Helical Navigation by Three-Dimensional Flagellar Beating,” *Phys. Rev. Lett.* **126**, 088003 (2021).
12. Knut Drescher, Kyriacos C. Leptos, Idan Tuval, Takuji Ishikawa, Timothy J. Pedley, and Raymond E. Goldstein, “Dancing volvox: Hydrodynamic bound states of swimming algae,” *Phys. Rev. Lett.* **102**, 168101 (2009).
13. Li Zhang, Jake J. Abbott, Lixin Dong, Bradley E. Kratochvil, Dominik Bell, and Bradley J. Nelson, “Artificial bacterial flagella: Fabrication and magnetic control,” *Appl. Phys. Lett.* **94**, 64107 (2009).
14. Ambarish Ghosh and Peer Fischer, “Controlled propulsion of artificial magnetic nanostructured propellers,” *Nano Lett.* **9**, 2243–2245 (2009).
15. Stefano Palagi and Peer Fischer, “Bioinspired microrobots,” *Nat. Rev. Mater.* **3**, 113–124 (2018).
16. J. G. Gibbs and P. Fischer, “Active colloidal microdrills,” *Chem. Commun.* **51**, 4192–4195 (2015).
17. Elsen Tjhung, Michael E. Cates, and Davide Marenduzzo, “Contractile and chiral activities codetermine the helicity of swimming droplet trajectories,” *Proc. Natl. Acad. Sci. U. S. A.* **114**, 4631–4636 (2017).
18. Livio Nicola Carenza, Giuseppe Gonnella, Davide Marenduzzo, and Giuseppe Negro, “Rotation and propulsion in 3D active chiral droplets,” *Proc. Natl. Acad. Sci.* **116**, 22065–22070 (2019).
19. Clemens Bechinger, Roberto Di Leonardo, Hartmut Löwen, Charles Reichhardt, Giorgio Volpe, and Giovanni Volpe, “Active Particles in Complex and Crowded Environments,” *Rev. Mod. Phys.* **88**, 045006 (2016).
20. Benno Liebchen and Demian Levis, “Chiral active matter,” *Europhys. Lett.* **139**, 67001 (2022).
21. Mark J. Bowick, Nikta Fakhri, M. Cristina Marchetti, and Sri-ram Ramaswamy, “Symmetry, Thermodynamics, and Topology in Active Matter,” *Phys. Rev. X* **12**, 010501 (2022).
22. Ingmar H. Riedel, Karsten Kruse, and Jonathon Howard, “A self-organized vortex array of hydrodynamically entrained sperm cells,” *Science* **309**, 300–303 (2005).
23. Eric Lauga, Willow R. DiLuzio, George M. Whitesides, and Howard A. Stone, “Swimming in Circles: Motion of Bacteria near Solid Boundaries,” *Biophys. J.* **90**, 400–412 (2006).
24. Alexander P. Petroff, Xiao Lun Wu, and Albert Libchaber, “Fast-moving bacteria self-organize into active two-dimensional crystals of rotating cells,” *Phys. Rev. Lett.* **114**, 158102 (2015).
25. He Li, Hugues Chaté, Masaki Sano, Xia-qing Shi, and H. P. Zhang, “Robust Edge Flows in Swarming Bacterial Colonies,” *Phys. Rev. X* **14**, 041006 (2024).
26. Igor S. Aranson, “Bacterial active matter,” *Reports Prog. Phys.* **85**, 076601 (2022).
27. Kyongwan Kim, Natsuhiko Yoshinaga, Sanjib Bhattacharyya, Hikaru Nakazawa, Mitsuo Umetsu, and Winfried Teizer, “Large-scale chirality in an active layer of microtubules and kinesin motor proteins,” *Soft Matter* **14**, 3221–3231 (2018).
28. Zuzana Dunajova, Batirtze Prats Mateu, Philipp Radler, Keesiang Lim, Dörte Brandis, Philipp Velicky, Johann Georg Danzl, Richard W. Wong, Jens Elgeti, Edouard Hannezo, and Martin Loose, “Chiral and nematic phases of flexible active filaments,” *Nat. Phys.* **19**, 1916–1926 (2023).
29. Felix Kümmel, Borge Ten Hagen, Raphael Wittkowski, Ivo Buttinoni, Ralf Eichhorn, Giovanni Volpe, Hartmut Löwen, and Clemens Bechinger, “Circular Motion of Asymmetric Self-Propelling Particles,” *Phys. Rev. Lett.* **110**, 198302 (2013).
30. Bartosz A. Grzybowski, Howard A. Stone, and George M. Whitesides, “Dynamic self-assembly of magnetized, millimetre-sized objects rotating at a liquid–air interface,” *Nature* **405**, 1033–1036 (2000).
31. Vishal Soni, Ephraim S. Bililign, Sofia Magkiriadou, Stefania Sacanna, Denis Bartolo, Michael J. Shelley, and William T. M. Irvine, “The odd free surface flows of a colloidal chiral fluid,” *Nat. Phys.* **15**, 1188–1194 (2019).
32. Antoine Bricard, Jean-Baptiste Caussin, Nicolas Desreumaux, Olivier Dauchot, and Denis Bartolo, “Emergence of macroscopic directed motion in populations of motile colloids,” *Nature* **503**, 95–98 (2013).
33. J. Elgeti, R. G. Winkler, and G. Gompper, “Physics of microswimmers—single particle motion and collective behavior: a review,” *Reports Prog. Phys.* **78**, 056601 (2015).
34. Eric Lauga, “Bacterial Hydrodynamics,” *Annu. Rev. Fluid Mech.* **48**, 105–130 (2016).
35. Leon Lettermann, Falko Ziebert, and Ulrich S. Schwarz, “A geometrical theory of gliding motility based on cell shape and surface flow,” *Proc. Natl. Acad. Sci.* **121**, e2410708121 (2024).
36. Christina L. Hueschen, Li-av Segev-Zarko, Jian-Hua Chen, Mark A. LeGros, Carolyn A. Larabell, John C. Boothroyd, Rob Phillips, and Alexander R. Dunn, “Emergent actin flows explain distinct modes of gliding motility,” *Nat. Phys.* , 1–8 (2024).
37. Pintu Patra, Konrad Beyer, Astha Jaiswal, Anna Battista, Karl Rohr, Friedrich Frischknecht, and Ulrich S. Schwarz, “Collective migration reveals mechanical flexibility of malaria parasites,” *Nat. Phys.* **18**, 586–594 (2022).
38. Katherine Copenhagen, Ricard Alert, Ned S. Wingreen, and Joshua W. Shaevitz, “Topological defects promote layer formation in Myxococcus xanthus colonies,” *Nat. Phys.* **17**, 211–215 (2021).
39. Endao Han, Chenyi Fei, Ricard Alert, Katherine Copenhagen, Matthias D. Koch, Ned S. Wingreen, and Joshua W. Shaevitz, “Local polar order controls mechanical stress and triggers layer formation in developing Myxococcus xanthus colonies,” , 1–35

- (2023), [arXiv:2308.00368](https://arxiv.org/abs/2308.00368).
40. M. C. Marchetti, J. F. Joanny, S. Ramaswamy, T. B. Liverpool, J. Prost, Madan Rao, and R. Aditi Simha, “Hydrodynamics of soft active matter,” *Rev. Mod. Phys.* **85**, 1143–1189 (2013).
 41. Markus Bär, Robert Großmann, Sebastian Heidenreich, and Fernando Peruani, “Self-Propelled Rods: Insights and Perspectives for Active Matter,” *Annu. Rev. Condens. Matter Phys.* **11**, 441–466 (2020).
 42. Julien Herrou and Târn Mignot, “Dynamic polarity control by a tunable protein oscillator in bacteria,” *Curr. Opin. Cell Biol.* **62**, 54–60 (2020).
 43. Quentin Vagne and Guillaume Salbreux, “Theory of cell aggregates as interacting, spinning, active polar particles,” (2024), [arXiv:2405.07540](https://arxiv.org/abs/2405.07540).
 44. Guannan Liu, Adam Patch, Fatmagül Bahar, David Yllanes, Roy D. Welch, M. Cristina Marchetti, Shashi Thutupalli, and Joshua W. Shaevitz, “Self-Driven Phase Transitions Drive Myxococcus xanthus Fruiting Body Formation,” *Phys. Rev. Lett.* **122**, 248102 (2019).
 45. Michael E. Cates and Julien Tailleur, “Motility-Induced Phase Separation,” *Annu. Rev. Condens. Matter Phys.* **6**, 219–244 (2015).
 46. Thomas Speck, “Collective forces in scalar active matter,” *Soft Matter* **16**, 2652–2663 (2020).
 47. Jie Zhang, Ricard Alert, Jing Yan, Ned S. Wingreen, and Steve Granick, “Active phase separation by turning towards regions of higher density,” *Nat. Phys.* **17**, 961–967 (2021).
 48. S. Ramaswamy, R. Aditi Simha, and J. Toner, “Active nematics on a substrate: Giant number fluctuations and long-time tails,” *Europhys. Lett.* **62**, 196–202 (2003).
 49. S. Fürthauer, M. Stempel, S. W. Grill, and F. Jülicher, “Active chiral fluids,” *Eur. Phys. J. E* **35**, 89 (2012).
 50. S. Fürthauer, M. Stempel, S. Grill, and F. Jülicher, “Active chiral processes in thin films,” *Phys. Rev. Lett.* **110**, 048103 (2013).
 51. Ananyo Maitra and Martin Lenz, “Spontaneous rotation can stabilise ordered chiral active fluids,” *Nat. Commun.* **10**, 920 (2019).
 52. Frank Jülicher, Stephan W Grill, and Guillaume Salbreux, “Hydrodynamic theory of active matter,” *Reports Prog. Phys.* **81**, 076601 (2018).
 53. Pavel Kraikivski, Reinhard Lipowsky, and Jan Kierfeld, “Enhanced ordering of interacting filaments by molecular motors,” *Phys. Rev. Lett.* **96**, 258103 (2006).
 54. Aparna Baskaran and M. Cristina Marchetti, “Enhanced diffusion and ordering of self-propelled rods,” *Phys. Rev. Lett.* **101**, 268101 (2008).
 55. Sreejith Santhosh, Mehrana R. Nejad, Amin Doostmohammadi, Julia M. Yeomans, and Sumesh P. Thampi, “Activity Induced Nematic Order in Isotropic Liquid Crystals,” *J. Stat. Phys.* **180**, 699–709 (2020).
 56. Benedikt Sabass, Matthias D Koch, Guannan Liu, Howard A Stone, and Joshua W Shaevitz, “Force generation by groups of migrating bacteria,” *Proc. Natl. Acad. Sci.* **114**, 7266–7271 (2017).
 57. Ludwig A. Hoffmann, Koen Schakenraad, Roeland M. H. Merks, and Luca Giomi, “Chiral stresses in nematic cell monolayers,” *Soft Matter* **16**, 764–774 (2020).
 58. V. Yashunsky, D. J. G. Pearce, C. Blanch-Mercader, F. Ascione, P. Silberzan, and L. Giomi, “Chiral Edge Current in Nematic Cell Monolayers,” *Phys. Rev. X* **12**, 041017 (2022).
 59. Kyogo Kawaguchi, Ryoichiro Kageyama, and Masaki Sano, “Topological defects control collective dynamics in neural progenitor cell cultures,” *Nature* **545**, 327–331 (2017).
 60. Antoine Barbot, Dominique Decanini, and Gilgueng Hwang, “Controllable Roll-to-Swim motion transition of helical nanoswimmers,” *IEEE Int. Conf. Intell. Robot. Syst.*, 4662–4667 (2014).
 61. Shashi Thutupalli, Mingzhai Sun, Filiz Bunyak, Kannappan Palaniappan, and Joshua W Shaevitz, “Directional reversals enable Myxococcus xanthus cells to produce collective one-dimensional streams during fruiting-body formation,” *J. R. Soc. Interface* **12**, 20150049 (2015).
 62. Céline Dinet, Alphée Michelot, Julien Herrou, and Târn Mignot, “Linking single-cell decisions to collective behaviours in social bacteria,” *Philos. Trans. R. Soc. B Biol. Sci.* **376**, 20190755 (2021).
 63. Abhishek Shrivastava, Visha K Patel, Yisha Tang, Susan Connolly Yost, Floyd E Dewhirst, and Howard C Berg, “Cargo transport shapes the spatial organization of a microbial community,” *Proc. Natl. Acad. Sci. U. S. A.* **115**, 8633–8638 (2018).
 64. Daisuke Nakane, Shoko Odaka, Kana Suzuki, and Takayuki Nishizaka, “Large-Scale Vortices with Dynamic Rotation Emerged from Monolayer Collective Motion of Gliding Flavobacteria,” *J. Bacteriol.* **203**, e00073–21 (2021).
 65. Suchismita Das, Matteo Ciarchi, Ziqi Zhou, Jing Yan, Jie Zhang, and Ricard Alert, “Flocking by Turning Away,” *Phys. Rev. X* **14**, 031008 (2024).

Supplementary Material

I. COARSE-GRAINING: FROM THE MICROSCOPIC MODEL TO A HYDRODYNAMIC DESCRIPTION

Here, we systematically coarse-grain the microscopic model for active screws, Eqs. (1) to (3), to derive the hydrodynamic equations describing their collective behavior. We repeat the Langevin equations of motion here for convenience:

$$\dot{\phi}_i = \omega \Phi_i(t) + \frac{\tau_i}{\xi_s}, \quad (\text{S1})$$

$$\frac{d\mathbf{r}_i}{dt} = \ell_{\parallel} \dot{\phi}_i \hat{\mathbf{n}}_i - \ell_{\perp} \dot{\phi}_i \boldsymbol{\epsilon} \cdot \hat{\mathbf{n}}_i + \frac{\mathbf{F}_i}{\xi_t}, \quad (\text{S2})$$

$$\frac{d\theta_i}{dt} = \frac{\Gamma_i}{\xi_r} + \eta_i^r(t), \quad (\text{S3})$$

The meaning of the different terms is explained in the Main Text. To perform the coarse-graining, we follow the derivations in Refs. ^{47,65} and extend them to include the spinning-rate variable specific to active screws.

A. Eliminating the equation of motion for the spinning rate

As explained in the Main Text, before starting the coarse-graining procedure, we eliminate Eq. (S1) by introducing it into Eq. (S2). This substitution, however, does not eliminate the spinning rate $\dot{\phi}_i$ as a degree of freedom, as $\dot{\phi}_i$ is still present in the spin torque transfer τ_i . In addition to the interaction term represented by τ_i , Eq. (S1) features the stochastic active driving term $\omega \Phi_i(t)$, which captures stochastic reversals of the self-propulsion direction. Such reversals were shown to give rise to an effective rotational diffusivity $D_r^{\text{eff}} = D_r + 2f_{\text{rev}}$, where f_{rev} is the average reversal frequency⁴⁴. Therefore, after eliminating Eq. (S1), the effective Langevin equations of motion for active screws reduce to

$$\frac{d\mathbf{r}_i}{dt} = \left[\omega + \frac{\tau_i}{\xi_s} \right] [\ell_{\parallel} \hat{\mathbf{n}}_i - \ell_{\perp} \boldsymbol{\epsilon} \cdot \hat{\mathbf{n}}_i] + \frac{\mathbf{F}_i}{\xi_t}, \quad (\text{S4})$$

$$\frac{d\theta_i}{dt} = \frac{\Gamma_i}{\xi_r} + \eta_i^{\text{r,eff}}(t), \quad (\text{S5})$$

where $\langle \eta_i^{\text{r,eff}}(t) \eta_j^{\text{r,eff}}(t') \rangle = 2D_r^{\text{eff}} \delta(t-t') \delta_{ij}$.

B. Smoluchowski equation and the BBGKY hierarchy

The behavior of the system encoded in the set of coupled Langevin equations Eqs. (S4) and (S5) can be equivalently described by the Smoluchowski equation for the N -particle distribution function $\Psi_N(\mathbf{r}_1, \hat{\mathbf{n}}_1, \dot{\phi}_1, \dots, \mathbf{r}_N, \hat{\mathbf{n}}_N, \dot{\phi}_N; t)$, which is the probability density of finding the N particles at positions $\mathbf{r}_1, \dots, \mathbf{r}_N$ with orientations $\hat{\mathbf{n}}_1, \dots, \hat{\mathbf{n}}_N$ and spinning at rates $\dot{\phi}_1, \dots, \dot{\phi}_N$ at time t :

$$\partial_t \Psi_N = - \sum_{i=1}^N [\nabla_i \cdot \mathbf{J}_{t,i} + \partial_{\theta_i} J_{r,i}]. \quad (\text{S6})$$

Here, \mathbf{J}_t and J_r are the translational and rotational probability currents, respectively, given by

$$\mathbf{J}_{t,i} = \left\{ \left[\omega + \frac{\tau_i}{\xi_s} \right] [\ell_{\parallel} \hat{\mathbf{n}}_i - \ell_{\perp} \boldsymbol{\epsilon} \cdot \hat{\mathbf{n}}_i] + \frac{\mathbf{F}_i}{\xi_t} \right\} \Psi_N, \quad (\text{S7a})$$

$$J_{r,i} = \frac{\Gamma_i}{\xi_r} \Psi_N - D_r^{\text{eff}} \partial_{\theta_i} \Psi_N. \quad (\text{S7b})$$

Note that the two-dimensional particle orientation $\hat{\mathbf{n}}_i$ is given in terms of the angle θ_i as $\hat{\mathbf{n}}_i = (\cos \theta_i, \sin \theta_i)^T$.

Integrating over the positions, orientations, and spinning rates of all particles but one, we obtain an equation for the one-particle distribution function $\Psi_1(\mathbf{r}_1, \theta_1, \dot{\phi}_1; t)$:

$$\begin{aligned} \partial_t \Psi_1 = & -\nabla_1 \cdot [\omega (\ell_{\parallel} \hat{\mathbf{n}}_1 - \ell_{\perp} \boldsymbol{\epsilon} \cdot \hat{\mathbf{n}}_1) \Psi_1] \\ & - \nabla_1 \cdot \left[(\ell_{\parallel} \hat{\mathbf{n}}_1 - \ell_{\perp} \boldsymbol{\epsilon} \cdot \hat{\mathbf{n}}_1) \frac{\tau_{\text{int}}}{\xi_s} \right] - \nabla_1 \cdot \frac{\mathbf{F}_{\text{int}}}{\xi_t} \\ & - \partial_{\theta_1} \frac{\Gamma_{\text{int}}}{\xi_r} + D_r^{\text{eff}} \partial_{\theta_1}^2 \Psi_1. \end{aligned} \quad (\text{S8})$$

Here, \mathbf{F}_{int} , Γ_{int} , and τ_{int} are the collective force, orientational torque, and spin torque, respectively, which encode the effects of interactions on particle 1. For pair-wise interactions, the collective force and torques can be expressed in terms of the two-particle distribution function $\Psi_2(\mathbf{r}_1, \theta_1, \dot{\phi}_1, \mathbf{r}_2, \theta_2, \dot{\phi}_2; t)$ as

$$\mathbf{F}_{\text{int}}(\mathbf{r}_1, \theta_1, \dot{\phi}_1; t) = \int d^2\mathbf{r}' d\theta' d\dot{\phi}' \mathbf{F}(\mathbf{r}' - \mathbf{r}_1, \theta' - \theta_1) \Psi_2(\mathbf{r}_1, \theta_1, \dot{\phi}_1, \mathbf{r}', \theta', \dot{\phi}'; t), \quad (\text{S9a})$$

$$\Gamma_{\text{int}}(\mathbf{r}_1, \theta_1, \dot{\phi}_1; t) = \int d^2\mathbf{r}' d\theta' d\dot{\phi}' \Gamma(\mathbf{r}' - \mathbf{r}_1, \theta' - \theta_1) \Psi_2(\mathbf{r}_1, \theta_1, \dot{\phi}_1, \mathbf{r}', \theta', \dot{\phi}'; t), \quad (\text{S9b})$$

$$\tau_{\text{int}}(\mathbf{r}_1, \theta_1, \dot{\phi}_1; t) = \int d^2\mathbf{r}' d\theta' d\dot{\phi}' \tau(\mathbf{r}' - \mathbf{r}_1, \theta' - \theta_1, \dot{\phi}' + \dot{\phi}_1) \Psi_2(\mathbf{r}_1, \theta_1, \dot{\phi}_1, \mathbf{r}', \theta', \dot{\phi}'; t). \quad (\text{S9c})$$

Here, $\mathbf{F}(\mathbf{r}, \theta)$, $\Gamma(\mathbf{r}, \theta)$, and $\tau(\mathbf{r}, \theta, \dot{\phi})$ are the force, orienta-

tion torque, and spin torque of interaction between the two

particles. These quantities depend on the relative coordinates $\mathbf{r} = \mathbf{r}' - \mathbf{r}_1$, $\theta = \theta' - \theta$, and $\dot{\phi} = \dot{\phi}' + \dot{\phi}_1$ of the interacting pair. With the assumptions discussed in the Main Text, the dependencies of the interaction forces and torques on the relative coordinates reduce to

$$\mathbf{F}(\mathbf{r}, \theta) = -F_r(r) \cos \theta \hat{\mathbf{r}}, \quad (\text{S10a})$$

$$\Gamma(\mathbf{r}, \theta) = \Gamma_r(r) \sin(2\theta), \quad (\text{S10b})$$

$$\tau(\mathbf{r}, \theta, \dot{\phi}) = \tau_r(r) \dot{\phi} \cos \theta, \quad (\text{S10c})$$

where the functions $F_r(r)$, $\Gamma_r(r)$, and $\tau_r(r)$ capture unspecified radial dependencies of the interactions, with $r = |\mathbf{r}|$ being the distance between the interacting particles.

With the collective force and torques given by Eq. (S9), Eq. (S8) is an integro-differential equation for Ψ_1 that involves Ψ_2 . Therefore, Eq. (S8) is the first equation in the BBGKY hierarchy. To truncate the hierarchy, we decompose Ψ_2 as

$$\begin{aligned} \Psi_2(\mathbf{r}_1, \theta_1, \dot{\phi}_1, \mathbf{r}', \theta', \dot{\phi}'; t) &= \Psi_1(\mathbf{r}', \theta', \dot{\phi}'; t) \\ &\times g(\mathbf{r}', \theta', \dot{\phi}' | \mathbf{r}_1, \theta_1, \dot{\phi}_1; t) \Psi_1(\mathbf{r}_1, \theta_1, \dot{\phi}_1; t). \end{aligned} \quad (\text{S11})$$

Here, $\Psi_2(\mathbf{r}_1, \theta_1, \dot{\phi}_1, \mathbf{r}', \theta', \dot{\phi}'; t)$ is the density of particle pairs with one particle with position \mathbf{r}_1 , orientation θ_1 , and spinning rate $\dot{\phi}_1$, and another particle with position \mathbf{r}' , orientation

θ' , and spinning rate $\dot{\phi}'$ at time t . Respectively, g is the dimensionless pair distribution function that encodes the conditional probability of finding a particle with position \mathbf{r}' , orientation θ' , and spinning rate $\dot{\phi}'$ given that another particle has position \mathbf{r}_1 , orientation θ_1 , and spinning rate $\dot{\phi}_1$. Introducing this decomposition into Eq. (S8) allows us to express it as a closed equation for Ψ_1 , hence closing the hierarchy. This closure goes beyond the molecular chaos approximation, as it keeps information about pair correlations in the pair distribution function g .

In homogeneous steady states, the probability distributions are time-independent, and the pair correlations do not depend on the coordinates of a given particle but only on the relative coordinates of particle pairs, defined just above Eq. (S10). Hence, we express g in terms of the distance r between particles, the angle φ formed between the interparticle distance vector \mathbf{r} and the orientation vector $\hat{\mathbf{n}}_1$ of particle 1 (defined by $\hat{\mathbf{n}}_1 \cdot \mathbf{r} = r \cos \varphi$), the relative orientation θ , and the relative spinning rate $\dot{\phi}$. Therefore, in homogeneous steady states like the nematic state of active screws that we analyze, we have

$$g(\mathbf{r}', \theta', \dot{\phi}' | \mathbf{r}_1, \theta_1, \dot{\phi}_1; t) = g(r, \varphi, \theta, \dot{\phi}). \quad (\text{S12})$$

With this decomposition, and changing the integration variables to the relative coordinates, the collective force and torques (Eq. (S9)) are expressed as

$$\mathbf{F}_{\text{int}}(\mathbf{r}_1, \theta_1, \dot{\phi}_1) = \Psi_1(\mathbf{r}_1, \theta_1, \dot{\phi}_1) \int d^2\mathbf{r} d\theta d\dot{\phi} \mathbf{F}(\mathbf{r}, \theta) \Psi_1(\mathbf{r} + \mathbf{r}_1, \theta + \theta_1, \dot{\phi} - \dot{\phi}_1) g(r, \varphi, \theta, \dot{\phi}), \quad (\text{S13a})$$

$$\Gamma_{\text{int}}(\mathbf{r}_1, \theta_1, \dot{\phi}_1) = \Psi_1(\mathbf{r}_1, \theta_1, \dot{\phi}_1) \int d^2\mathbf{r} d\theta d\dot{\phi} \Gamma(\mathbf{r}, \theta) \Psi_1(\mathbf{r} + \mathbf{r}_1, \theta + \theta_1, \dot{\phi} - \dot{\phi}_1) g(r, \varphi, \theta, \dot{\phi}), \quad (\text{S13b})$$

$$\tau_{\text{int}}(\mathbf{r}_1, \theta_1, \dot{\phi}_1) = \Psi_1(\mathbf{r}_1, \theta_1, \dot{\phi}_1) \int d^2\mathbf{r} d\theta d\dot{\phi} \tau(\mathbf{r}, \theta, \dot{\phi}) \Psi_1(\mathbf{r} + \mathbf{r}_1, \theta + \theta_1, \dot{\phi} - \dot{\phi}_1) g(r, \varphi, \theta, \dot{\phi}). \quad (\text{S13c})$$

C. Fourier and gradient expansions

The one-particle distribution function Ψ_1 in the integrand of Eq. (S13) introduces non-local dependencies in \mathbf{r}_1 , θ_1 , and $\dot{\phi}_1$. To derive local hydrodynamic equations, we perform a Fourier expansion on the orientation angle,

$$\Psi_1(\mathbf{r}', \theta', \dot{\phi}') = \frac{1}{2\pi} \sum_{k=0}^{\infty} e^{-ik\theta'} \tilde{\Psi}_{1,k}(\mathbf{r}', \dot{\phi}'), \quad (\text{S14})$$

and then a gradient expansion of the Fourier components on both the position and the spinning rate,

$$\begin{aligned} \tilde{\Psi}_{1,k}(\mathbf{r}', \dot{\phi}') &\approx \tilde{\Psi}_{1,k}(\mathbf{r}_1, \dot{\phi}_1) + (\mathbf{r}' - \mathbf{r}_1) \cdot \nabla_{\mathbf{r}'} \tilde{\Psi}_{1,k}(\mathbf{r}_1, \dot{\phi}_1) \\ &+ (\dot{\phi}' - \dot{\phi}_1) \partial_{\dot{\phi}'} \tilde{\Psi}_{1,k}(\mathbf{r}_1, \dot{\phi}_1). \end{aligned} \quad (\text{S15})$$

The arguments in these expressions relate to those of Ψ_1 in the integrand of Eq. (S13) via the transformations to the relative coordinates: $\mathbf{r} = \mathbf{r}' - \mathbf{r}_1$, $\theta = \theta' - \theta$, and $\dot{\phi} = \dot{\phi}' + \dot{\phi}_1$.

1. Zeroth-order contributions

Based on this gradient expansion, we now obtain first the zeroth-order and then the first-order contributions to the collective interaction force and torques in Eq. (S13). The interaction force is a vector, which we take to be along the interparticle distance axis $\hat{\mathbf{r}}$, as in Eq. (S10a). We then decompose it into components parallel and perpendicular to the orientation of particle 1: $\hat{\mathbf{r}} = \cos \varphi \hat{\mathbf{n}}_1 + \sin \varphi \hat{\mathbf{t}}_1$, where $\hat{\mathbf{t}}_1$ is unit vector transverse to $\hat{\mathbf{n}}_1$, which thus fulfills $\hat{\mathbf{t}}_1 \cdot \hat{\mathbf{n}}_1 = 0$. Using this decomposition in Eq. (S13a), the zeroth-order contributions of Eq. (S13) are given by

$$F_{\text{int},\parallel}^{(0)}(\mathbf{r}_1, \theta_1, \dot{\phi}_1) = -\Psi_1(\mathbf{r}_1, \theta_1, \dot{\phi}_1) \frac{1}{2\pi} \sum_{k=0}^{\infty} e^{-ik\theta_1} \tilde{\Psi}_{1,k}(\mathbf{r}_1, \dot{\phi}_1) \zeta_{0,k}^{\parallel}, \quad (\text{S16a})$$

$$F_{\text{int},\perp}^{(0)}(\mathbf{r}_1, \theta_1, \dot{\phi}_1) = -\Psi_1(\mathbf{r}_1, \theta_1, \dot{\phi}_1) \frac{1}{2\pi} \sum_{k=0}^{\infty} e^{-ik\theta_1} \tilde{\Psi}_{1,k}(\mathbf{r}_1, \dot{\phi}_1) \zeta_{0,k}^{\perp}, \quad (\text{S16b})$$

$$\Gamma_{\text{int}}^{(0)}(\mathbf{r}_1, \theta_1, \dot{\phi}_1) = \Psi_1(\mathbf{r}_1, \theta_1, \dot{\phi}_1) \frac{1}{2\pi} \sum_{k=0}^{\infty} e^{-ik\theta_1} \tilde{\Psi}_{1,k}(\mathbf{r}_1, \dot{\phi}_1) \gamma_{0,k}, \quad (\text{S16c})$$

$$\tau_{\text{int}}^{(0)}(\mathbf{r}_1, \theta_1, \dot{\phi}_1) = \Psi_1(\mathbf{r}_1, \theta_1, \dot{\phi}_1) \frac{1}{2\pi} \sum_{k=0}^{\infty} e^{-ik\theta_1} \tilde{\Psi}_{1,k}(\mathbf{r}_1, \dot{\phi}_1) \tau_{0,k}, \quad (\text{S16d})$$

where we have defined the coefficients

$$\zeta_{0,k}^{\parallel} \equiv \int_0^{\infty} dr r \int_0^{2\pi} d\varphi \int_0^{2\pi} d\theta \int_{-\infty}^{\infty} d\dot{\phi} F(r, \varphi, \theta) g(r, \varphi, \theta, \dot{\phi}) \cos \varphi e^{-ik\theta}, \quad (\text{S17a})$$

$$\zeta_{0,k}^{\perp} \equiv \int_0^{\infty} dr r \int_0^{2\pi} d\varphi \int_0^{2\pi} d\theta \int_{-\infty}^{\infty} d\dot{\phi} F(r, \varphi, \theta) g(r, \varphi, \theta, \dot{\phi}) \sin \varphi e^{-ik\theta}, \quad (\text{S17b})$$

$$\gamma_{0,k} \equiv \int_0^{\infty} dr r \int_0^{2\pi} d\varphi \int_0^{2\pi} d\theta \int_{-\infty}^{\infty} d\dot{\phi} \Gamma(r, \varphi, \theta) g(r, \varphi, \theta, \dot{\phi}) e^{-ik\theta}, \quad (\text{S17c})$$

$$\tau_{0,k} \equiv \int_0^{\infty} dr r \int_0^{2\pi} d\varphi \int_0^{2\pi} d\theta \int_{-\infty}^{\infty} d\dot{\phi} \tau(r, \varphi, \theta, \dot{\phi}) g(r, \varphi, \theta, \dot{\phi}) e^{-ik\theta}. \quad (\text{S17d})$$

Next, we simplify these expressions through three assumptions:

- (i) We introduce the specific forms of the interaction force and torques given in Eq. (S10).
- (ii) We assume that the entire system is non-chiral, as half of the screws will spin in one sense and half of the screws in the other. Hence, the pair correlation function has to be invariant upon chiral transformations, i.e. simultaneous change of sign of the angles φ and θ , $g(r, -\varphi, -\theta, \dot{\phi}) = g(r, \varphi, \theta, \dot{\phi})$, and upon change of sign of the spinning rate $\dot{\phi}$, $g(r, \varphi, \theta, -\dot{\phi}) = g(r, \varphi, \theta, \dot{\phi})$.
- (iii) We consider the system of active screws to be deep in the nematic state. In this state, the orientation differences between pairs of particles are very small and, hence, the pair correlation function is sharply peaked around $\theta = 0$: $g(r, \varphi, \theta, \dot{\phi}) \approx g_{\text{nem}}(r, \varphi, \dot{\phi}) \delta(\theta)$.

With these assumptions, we get that $\zeta_{0,k}^{\parallel}$ does not vanish and

it is given by

$$\zeta_0 = \int_0^{\infty} dr r \int_0^{2\pi} d\varphi \int_{-\infty}^{\infty} d\dot{\phi} F_r(r) g_{\text{nem}}(r, \varphi, \dot{\phi}) \cos \varphi, \quad (\text{S18})$$

Here, we have renamed $\zeta_{0,k}^{\parallel} \rightarrow \zeta_0$ using that this coefficient is now independent of k . The other coefficients in Eq. (S17) vanish: $\zeta_{0,k}^{\perp} = 0$, $\gamma_{0,k} = 0$, and $\tau_{0,k} = 0$.

Therefore, summarizing the results at zeroth order in the gradient expansion, specified for the nematic state, we have

$$\mathbf{F}_{\text{int}}^{(0)} = -\Psi_1^2 \zeta_0 \hat{\mathbf{n}}_1, \quad (\text{S19a})$$

$$\Gamma_{\text{int}}^{(0)} = 0, \quad (\text{S19b})$$

$$\tau_{\text{int}}^{(0)} = 0. \quad (\text{S19c})$$

2. First-order contributions

We now obtain the first-order contributions to the collective interaction force and torques in Eq. (S13). We proceed as for the zeroth-order terms, except that we now also split the spatial gradients in components parallel and perpendicular to $\hat{\mathbf{n}}_1$. Thus, we obtain

$$F_{\text{int},\parallel}^{(1)}(\mathbf{r}_1, \theta_1, \dot{\phi}_1) = -\Psi_1(\mathbf{r}_1, \theta_1, \dot{\phi}_1) \frac{1}{2\pi} \sum_{k=0}^{\infty} e^{-ik\theta_1} \left[\zeta_{1,k,\parallel}^{\parallel} \nabla_{\parallel} + \zeta_{1,k,\perp}^{\parallel} \nabla_{\perp} + \zeta_{1,k,\dot{\phi}}^{\parallel} \partial_{\dot{\phi}} \right] \tilde{\Psi}_{1,k}(\mathbf{r}_1, \dot{\phi}_1), \quad (\text{S20a})$$

$$F_{\text{int},\perp}^{(1)}(\mathbf{r}_1, \theta_1, \dot{\phi}_1) = -\Psi_1(\mathbf{r}_1, \theta_1, \dot{\phi}_1) \frac{1}{2\pi} \sum_{k=0}^{\infty} e^{-ik\theta_1} \left[\zeta_{1,k,\parallel}^{\perp} \nabla_{\parallel} + \zeta_{1,k,\perp}^{\perp} \nabla_{\perp} + \zeta_{1,k,\dot{\phi}}^{\perp} \partial_{\dot{\phi}} \right] \tilde{\Psi}_{1,k}(\mathbf{r}_1, \dot{\phi}_1), \quad (\text{S20b})$$

$$\Gamma_{\text{int}}^{(0)}(\mathbf{r}_1, \theta_1, \dot{\phi}_1) = \Psi_1(\mathbf{r}_1, \theta_1, \dot{\phi}_1) \frac{1}{2\pi} \sum_{k=0}^{\infty} e^{-ik\theta_1} \left[\gamma_{1,k,\parallel} \nabla_{\parallel} + \gamma_{1,k,\perp} \nabla_{\perp} + \gamma_{1,k,\dot{\phi}} \partial_{\dot{\phi}} \right] \tilde{\Psi}_{1,k}(\mathbf{r}_1, \dot{\phi}_1), \quad (\text{S20c})$$

$$\tau_{\text{int}}^{(0)}(\mathbf{r}_1, \theta_1, \dot{\phi}_1) = \Psi_1(\mathbf{r}_1, \theta_1, \dot{\phi}_1) \frac{1}{2\pi} \sum_{k=0}^{\infty} e^{-ik\theta_1} \left[\tau_{1,k,\parallel} \nabla_{\parallel} + \tau_{1,k,\perp} \nabla_{\perp} + \tau_{1,k,\dot{\phi}} \partial_{\dot{\phi}} \right] \tilde{\Psi}_{1,k}(\mathbf{r}_1, \dot{\phi}_1), \quad (\text{S20d})$$

where we have defined the coefficients

$$\zeta_{1,k,\parallel}^{\parallel} \equiv \int_0^{\infty} dr r \int_0^{2\pi} d\varphi \int_0^{2\pi} d\theta \int_{-\infty}^{\infty} d\dot{\phi} F(r, \varphi, \theta) g(r, \varphi, \theta, \dot{\phi}) r \cos^2 \varphi e^{-ik\theta}, \quad (\text{S21a})$$

$$\zeta_{1,k,\perp}^{\parallel} \equiv \int_0^{\infty} dr r \int_0^{2\pi} d\varphi \int_0^{2\pi} d\theta \int_{-\infty}^{\infty} d\dot{\phi} F(r, \varphi, \theta) g(r, \varphi, \theta, \dot{\phi}) r \cos \varphi \sin \varphi e^{-ik\theta}, \quad (\text{S21b})$$

$$\zeta_{1,k,\dot{\phi}}^{\parallel} \equiv \int_0^{\infty} dr r \int_0^{2\pi} d\varphi \int_0^{2\pi} d\theta \int_{-\infty}^{\infty} d\dot{\phi} F(r, \varphi, \theta) g(r, \varphi, \theta, \dot{\phi}) \dot{\phi} \cos \varphi e^{-ik\theta}, \quad (\text{S21c})$$

$$\zeta_{1,k,\parallel}^{\perp} \equiv \int_0^{\infty} dr r \int_0^{2\pi} d\varphi \int_0^{2\pi} d\theta \int_{-\infty}^{\infty} d\dot{\phi} F(r, \varphi, \theta) g(r, \varphi, \theta, \dot{\phi}) r \sin \varphi \cos \varphi e^{-ik\theta}, \quad (\text{S21d})$$

$$\zeta_{1,k,\perp}^{\perp} \equiv \int_0^{\infty} dr r \int_0^{2\pi} d\varphi \int_0^{2\pi} d\theta \int_{-\infty}^{\infty} d\dot{\phi} F(r, \varphi, \theta) g(r, \varphi, \theta, \dot{\phi}) r \sin^2 \varphi e^{-ik\theta}, \quad (\text{S21e})$$

$$\zeta_{1,k,\dot{\phi}}^{\perp} \equiv \int_0^{\infty} dr r \int_0^{2\pi} d\varphi \int_0^{2\pi} d\theta \int_{-\infty}^{\infty} d\dot{\phi} F(r, \varphi, \theta) g(r, \varphi, \theta, \dot{\phi}) \dot{\phi} \sin \varphi e^{-ik\theta}, \quad (\text{S21f})$$

$$\gamma_{1,k,\parallel} \equiv \int_0^{\infty} dr r \int_0^{2\pi} d\varphi \int_0^{2\pi} d\theta \int_{-\infty}^{\infty} d\dot{\phi} \Gamma(r, \varphi, \theta) g(r, \varphi, \theta, \dot{\phi}) r \cos \varphi e^{-ik\theta}, \quad (\text{S21g})$$

$$\gamma_{1,k,\perp} \equiv \int_0^{\infty} dr r \int_0^{2\pi} d\varphi \int_0^{2\pi} d\theta \int_{-\infty}^{\infty} d\dot{\phi} \Gamma(r, \varphi, \theta) g(r, \varphi, \theta, \dot{\phi}) r \sin \varphi e^{-ik\theta}, \quad (\text{S21h})$$

$$\gamma_{1,k,\dot{\phi}} \equiv \int_0^{\infty} dr r \int_0^{2\pi} d\varphi \int_0^{2\pi} d\theta \int_{-\infty}^{\infty} d\dot{\phi} \Gamma(r, \varphi, \theta) g(r, \varphi, \theta, \dot{\phi}) \dot{\phi} e^{-ik\theta}, \quad (\text{S21i})$$

$$\tau_{1,k,\parallel} \equiv \int_0^{\infty} dr r \int_0^{2\pi} d\varphi \int_0^{2\pi} d\theta \int_{-\infty}^{\infty} d\dot{\phi} \tau(r, \varphi, \theta, \dot{\phi}) g(r, \varphi, \theta, \dot{\phi}) r \cos \varphi e^{-ik\theta}, \quad (\text{S21j})$$

$$\tau_{1,k,\perp} \equiv \int_0^{\infty} dr r \int_0^{2\pi} d\varphi \int_0^{2\pi} d\theta \int_{-\infty}^{\infty} d\dot{\phi} \tau(r, \varphi, \theta, \dot{\phi}) g(r, \varphi, \theta, \dot{\phi}) r \sin \varphi e^{-ik\theta}, \quad (\text{S21k})$$

$$\tau_{1,k,\dot{\phi}} \equiv \int_0^{\infty} dr r \int_0^{2\pi} d\varphi \int_0^{2\pi} d\theta \int_{-\infty}^{\infty} d\dot{\phi} \tau(r, \varphi, \theta, \dot{\phi}) g(r, \varphi, \theta, \dot{\phi}) \dot{\phi} e^{-ik\theta}. \quad (\text{S21l})$$

Here, as in the zeroth-order terms, the \parallel and \perp superscripts refer to the components of the collective force \mathbf{F}_{int} parallel and perpendicular to $\hat{\mathbf{n}}_1$. Respectively, the \parallel , \perp , and $\dot{\phi}$ subscripts refer to the components of the spatial gradients parallel and perpendicular to $\hat{\mathbf{n}}_1$, ∇_{\parallel} and ∇_{\perp} , and to the spinning-rate gradient $\partial_{\dot{\phi}}$ in Eq. (S20).

We now simplify these expressions using the same three assumptions as for the zeroth-order coefficients, listed after

Eq. (S17). We thus obtain

$$\zeta_{1,\parallel}^{\parallel} = \int_0^{\infty} dr \int_0^{2\pi} d\varphi \int_{-\infty}^{\infty} d\dot{\phi} F_r(r) g_{\text{nem}}(r, \varphi, \dot{\phi}) r^2 \cos^2 \varphi, \quad (\text{S22a})$$

$$\zeta_{1,\perp}^{\perp} = \int_0^{\infty} dr \int_0^{2\pi} d\varphi \int_{-\infty}^{\infty} d\dot{\phi} F_r(r) g_{\text{nem}}(r, \varphi, \dot{\phi}) r^2 \sin^2 \varphi, \quad (\text{S22b})$$

$$\tau_{1,\dot{\phi}} = \int_0^{\infty} dr \int_0^{2\pi} d\varphi \int_{-\infty}^{\infty} d\dot{\phi} \tau_r(r) g_{\text{nem}}(r, \varphi, \dot{\phi}) r \dot{\phi}^2, \quad (\text{S22c})$$

where we have dropped the subindex k because these coefficients are now independent of the angular mode number. The rest of coefficients in Eq. (S21) vanish. The integrals in the expressions of $\zeta_{1,k,\parallel}^{\parallel}$ and $\zeta_{1,k,\perp}^{\perp}$ are different but, for typical forms of the pair correlation function, they take similar values. For simplicity, following previous work⁴⁷, we replace these integrals by their average, thus replacing both $\zeta_{1,k,\parallel}^{\parallel}$ and $\zeta_{1,k,\perp}^{\perp}$ by

$$\zeta_1 \equiv \frac{1}{2} \int_0^\infty dr \int_0^{2\pi} d\varphi \int_{-\infty}^\infty d\dot{\phi} F_r(r) g_{\text{nem}}(r, \varphi, \dot{\phi}) r^2. \quad (\text{S23})$$

Summarizing the results at first order in the gradient expansion, specified for the nematic state, we have

$$\mathbf{F}_{\text{int}}^{(1)} = -\Psi_1 \zeta_1 \nabla \Psi_1, \quad (\text{S24a})$$

$$\Gamma_{\text{int}}^{(1)} = 0, \quad (\text{S24b})$$

$$\tau_{\text{int}}^{(1)} = \Psi_1 \tau_{1,\dot{\phi}} \partial_{\dot{\phi}} \Psi_1. \quad (\text{S24c})$$

Finally, putting together the zeroth- and first-order terms, the collective force and torques representing the effects of interactions on a reference particle in the nematic state read

$$\mathbf{F}_{\text{int}} = -\Psi_1^2 \zeta_0 \hat{\mathbf{n}}_1 - \Psi_1 \zeta_1 \nabla \Psi_1, \quad (\text{S25a})$$

$$\Gamma_{\text{int}} = 0, \quad (\text{S25b})$$

$$\tau_{\text{int}} = \Psi_1 \tau_{1,\dot{\phi}} \partial_{\dot{\phi}} \Psi_1. \quad (\text{S25c})$$

D. Moment hierarchy and hydrodynamic equations

To complete the coarse-graining of the microscopic model, we define continuum fields as the angular moments of the one-particle distribution function Ψ_1 . For example, the zeroth moment corresponds to the density field $\rho(\mathbf{r}, t)$, the first moment corresponds to the polarization density $\mathbf{p}(\mathbf{r}, t)$, and the second moment is related to the nematic order-parameter tensor density $\mathbf{Q}(\mathbf{r}, t)$:

$$\rho(\mathbf{r}, t) = \int \Psi_1(\mathbf{r}, \theta, \dot{\phi}, t) d\theta d\dot{\phi}, \quad (\text{S26a})$$

$$p_\alpha(\mathbf{r}, t) = \int n_\alpha \Psi_1(\mathbf{r}, \theta, \dot{\phi}, t) d\theta d\dot{\phi}, \quad (\text{S26b})$$

$$Q_{\alpha\beta}(\mathbf{r}, t) = \int \left[n_\alpha n_\beta - \frac{1}{2} \delta_{\alpha\beta} \right] \Psi_1(\mathbf{r}, \theta, \dot{\phi}, t) d\theta d\dot{\phi}. \quad (\text{S26c})$$

We can then obtain hydrodynamic equations for each of these fields by taking the corresponding moment of the Smoluchowski equation Eq. (S8) for the one-particle distribution Ψ_1 , completed with the collective force and torques given in Eq. (S25). When integrating the terms containing two factors of Ψ_1 in Eq. (S25a), we assume that they factor out and give rise to nonlinear terms in the hydrodynamic fields. For example, the term that goes like $\Psi_1^2 \hat{\mathbf{n}}_1$ in Eq. (S25a) coarse-grains to a nonlinear term like $\rho \mathbf{p}$. Proceeding in this way, we obtain

the following equations for the density, polarity, and nematic order-parameter fields:

$$\partial_t \rho = -\nabla \cdot \mathbf{J}; \quad \mathbf{J} = v_{\parallel}[\rho] \mathbf{p} - v_{\perp} \boldsymbol{\epsilon} \cdot \mathbf{p} - \zeta_1 \rho \nabla \rho, \quad (\text{S27a})$$

$$\begin{aligned} \partial_t \mathbf{p} = & -\nabla \cdot (v_{\parallel}[\rho] \mathbf{Q}) - \frac{1}{2} \nabla (v_{\parallel}[\rho] \rho) + \nabla \cdot (v_{\perp} \boldsymbol{\epsilon} \cdot \mathbf{Q}) \\ & + \frac{1}{2} \boldsymbol{\epsilon} \cdot \nabla (v_{\perp} \rho) + \nabla \cdot (\zeta_1 \mathbf{p} \nabla \rho) - D_r^{\text{eff}} \mathbf{p}, \end{aligned} \quad (\text{S27b})$$

$$\begin{aligned} \partial_t Q_{\alpha\beta} = & -\partial_\gamma (v_{\parallel}[\rho] T_{\alpha\beta\gamma}) + \delta_{\alpha\beta} \partial_\gamma \left(\frac{v_{\parallel}[\rho]}{2} p_\gamma \right) \\ & + \partial_\gamma (v_{\perp} \epsilon_{\gamma\mu} T_{\alpha\beta\mu}) - \partial_\gamma \left(\frac{v_{\perp}}{2} \delta_{\alpha\beta} \epsilon_{\gamma\mu} p_\mu \right) \\ & + \partial_\gamma (\zeta_1 Q_{\alpha\beta} \partial_\gamma \rho) - D_r^{\text{eff}} Q_{\alpha\beta}, \end{aligned} \quad (\text{S27c})$$

are quoted in Eqs. (4), (5) and (8) in the Main Text. These hydrodynamic equations, together with the definitions

$$v_{\parallel}[\rho] = \omega \ell_{\parallel} - \zeta_0 \rho, \quad (\text{S28a})$$

$$v_{\perp} = \omega \ell_{\perp}, \quad (\text{S28b})$$

$$D_r^{\text{eff}} = D_r + 2f_{\text{rev}}, \quad (\text{S28c})$$

and the results for ζ_0 and ζ_1 in Eqs. (S18) and (S23), constitute the final result of our derivation. They specify the collective behavior of the system of active screws in terms of the parameters of their microscopic model, complemented with the pair correlation function in the nematic state, g_{nem} , needed to obtain ζ_0 and ζ_1 .

In general, the hydrodynamic equation for the k^{th} moment involves the $k + 1^{\text{th}}$ moment, giving rise to a hierarchy of hydrodynamic equations. In Eq. (S27), the equation for the nematic order parameter contains the third-rank orientational tensor

$$T_{\alpha\beta\gamma}(\mathbf{r}, t) = \int n_\alpha n_\beta n_\gamma \Psi_1(\mathbf{r}, \theta, \dot{\phi}, t) d\theta d\dot{\phi}, \quad (\text{S29})$$

which is the third-order orientational moment of Ψ_1 . Here, we consider only the first three equations of the hierarchy (Eq. (S27)).

II. FLOW FIELDS AROUND TOPOLOGICAL DEFECTS

We analyze the flows of *M. xanthus* bacteria around +1/2 topological defects reported in Fig. 4 of Ref.³⁸. To reveal the presence of chiral flows, we compute the average velocity in a circle of radius R around the defect. For $R = 5 \mu\text{m}$, we obtain $\langle v_x \rangle_{R=5 \mu\text{m}} = -0.599(3) \mu\text{m}/\text{min}$ and $\langle v_y \rangle_{R=5 \mu\text{m}} = 0.113(2) \mu\text{m}/\text{min}$. For $R = 10 \mu\text{m}$, we obtain $\langle v_x \rangle_{R=10 \mu\text{m}} = -0.354(3) \mu\text{m}/\text{min}$ and $\langle v_y \rangle_{R=10 \mu\text{m}} = 0.0521(9) \mu\text{m}/\text{min}$. Errors are the standard errors of the mean. From these results, we obtain the ratio of velocity components quoted in the Main Text.

To compare these measurements to the theoretical predictions, we solve Eq. (6) around a +1/2 topological defect. Following Refs.^{38,59}, we also include anisotropic friction via a

friction coefficient matrix $\xi_{\alpha\beta} = \xi_0(\delta_{\alpha\beta} - \varepsilon Q_{\alpha\beta})$, where ε is the friction anisotropy, not to be confused with the Levi-Civita symbol ϵ used to obtain chiral components in the Main Text. The predicted flow fields read

$$v_x^+(r, \phi) = -\frac{\zeta}{\xi_0} \left[S'(r) + \frac{S(r)}{r} \right] \frac{1 + \varepsilon S(r) \cos \phi}{1 - \varepsilon^2 S^2(r)} + \frac{\zeta_c}{\xi_0} \left[S'(r) + \frac{S(r)}{r} \right] \frac{\varepsilon S(r) \sin \phi}{1 - \varepsilon^2 S^2(r)}, \quad (\text{S30a})$$

$$v_y^+(r, \phi) = -\frac{\zeta}{\xi_0} \left[S'(r) + \frac{S(r)}{r} \right] \frac{\varepsilon S(r) \sin \phi}{1 - \varepsilon^2 S^2(r)} - \frac{\zeta_c}{\xi_0} \left[S'(r) + \frac{S(r)}{r} \right] \frac{1 + \varepsilon S(r) \cos \phi}{1 - \varepsilon^2 S^2(r)}. \quad (\text{S30b})$$

Here, the + superscript indicates the positive defect charge, and the result is given in the polar coordinates r and ϕ . For a +1/2 defect, the nematic orientation angle is $\theta = \phi/2$. Respectively, $S(r)$ is the strength of nematic order. It can be approximated by the following Padé approximant³⁸

$$S(r) = S_0 f(r/\ell); \quad f(x) \approx x \sqrt{\frac{0.34 + 0.07x^2}{1 + 0.41x^2 + 0.07x^4}}, \quad (\text{S31})$$

where S_0 is the strength of the nematic order away from the defect, and ℓ is the nematic healing length, which determines the defect core size. We plot Eq. (S30) in Fig. 3a.

Averaging the flow field over the polar angle ϕ , we obtain

$$\langle v_x^+(r) \rangle_\phi = -\frac{\zeta}{\xi_0} \left[S'(r) + \frac{S(r)}{r} \right] \frac{1}{1 - \varepsilon^2 S^2(r)}, \quad (\text{S32a})$$

$$\langle v_y^+(r) \rangle_\phi = -\frac{\zeta_c}{\xi_0} \left[S'(r) + \frac{S(r)}{r} \right] \frac{1}{1 - \varepsilon^2 S^2(r)}. \quad (\text{S32b})$$

The ratio of these expressions is independent of both the radial coordinate r and of the friction anisotropy ε . Therefore, the ratio of the average velocity components in a circle of any radius R around the defect is given by

$$\frac{\langle v_y^+ \rangle_R}{\langle v_x^+ \rangle_R} = \frac{\zeta_c}{\zeta}. \quad (\text{S33})$$

We use this result to estimate the ratio of the chiral to non-chiral activity in the Main Text.

For completeness, we also compute the flow field around -1/2 defects, with a nematic orientation angle $\theta = -\phi/2$. We obtain

$$v_x^-(r, \phi) = -\frac{\zeta}{\xi_0} \left[S'(r) - \frac{S(r)}{r} \right] \times \frac{[1 + \varepsilon S(r) \cos \phi] \cos 2\phi + \varepsilon S(r) \sin \phi \sin 2\phi}{1 - \varepsilon^2 S^2(r)} \quad (\text{S34a})$$

$$+ \frac{\zeta_c}{\xi_0} \left[S'(r) - \frac{S(r)}{r} \right] \frac{(2 \cos \phi - \varepsilon S(r)) \sin \phi}{1 - \varepsilon^2 S^2(r)},$$

$$v_y^-(r, \phi) = \frac{\zeta}{\xi_0} \left[S'(r) - \frac{S(r)}{r} \right] \frac{(2 \cos \phi - \varepsilon S(r)) \sin \phi}{1 - \varepsilon^2 S^2(r)} - \frac{\zeta_c}{\xi_0} \left[S'(r) - \frac{S(r)}{r} \right] \times \frac{[1 + \varepsilon S(r) \cos \phi] \cos 2\phi + \varepsilon S(r) \sin \phi \sin 2\phi}{1 - \varepsilon^2 S^2(r)}, \quad (\text{S34b})$$

which we plot in Fig. 3b.